Master's Thesis

Multi-dimensional Carbon Nanomaterials for Supercapacitors

Jin-Wook Min

Department of Chemical Engineering

Graduate School of UNIST

2018

Multi-dimensional Carbon Nanomaterials for Supercapacitors

Jin-Wook Min

Department of Chemical Engineering

Graduate School of UNIST

Multi-dimensional Carbon Nanomaterials for Supercapacitors

A thesis/dissertation

submitted to the Graduate School of UNIST

in partial fulfillment of the

requirements for the degree of

Master of Science

Jin-Wook Min

06. 26. 2018

Approved by

_____

Advisor

Ji-Hyun Jang

Multi-dimensional Carbon Nanomaterials for Supercapacitors

Jin-Wook Min

This certifies that the thesis/dissertation of Jin-Wook Min is approved.

06. 26. 2018

Signature

_____

Advisor: Ji-Hyun Jang

Signature

_____

Hyun-Kon Song

Signature

_____

Jongnam Park

Table of Contents

List of Figures

Abstract

In recent years, Wearable electronics attracted substantial amount of popularity due to their seamless addition to every human life. These devices could be attached onto anywhere, which directly attached onto human skin for application such as portable, sensors on the clothes, and self-powered electronics. Usually, the fabrication of wearable devices involved by electroplating, vacuum deposition, photolithography, etc. However the previous method is drawbacks including many step process, environmental undesirable waste and high-cost. In order to solve these disadvantages, the printing technologies is a suitable alternative due to easy approach, facile and scalable fabrication and controlled thickness and uniformity of the film. Wearable energy storage devices show promising results indicate that has outstanding potential in a various range of wearable electronics.

At this paper, the study by various Three Dimensionally(3D) active materials and the applications are described using 3D graphene nanonetworks(3DGNs) and metal oxides/hydroxides. Among many applications, we studied to fabricate printable supercapacitors (SCs) using inkjet printing at first. Most of supercapacitors could be differentiated, depending on the active materials as well as the mechanism of charge storage procedure. Electric Double Layer Capacitors (EDLC) are the main stream devices at present. Therefore, the carbon allotrope as active materials of the EDLC that are high electrochemical stability and has high surface area. We focus on making 3DGNs for a huge surface area and high efficiency capacitance by using active materials. Conducting Single Wall Carbon Nanotube (SWCNT) and Ag nanowire ink printed on the A4 substrate several times so that it is used as current collector. Printed two types of electrodes are used interconnected 3D Graphene Nano-networks (i-3DGNs) as the anode and i-3DGNs / Manganese oxide (MnO_2) as the cathode. Mixed SWCNT established hierarchical short, long-range electron and ion passage. To assemble asymmetric supercapacitor (ASC), poly (vinyl alcohol) (PVA)-LiCl gel polymer electrolyte is covered on negative and positive electrode. The printed ASC shows excellent flexibility, nice cycle stability and improved energy density and wide potential window of 0-2V. Because the electrochemical performance was transformed through control the number of printing layer and design of texts, versatility of inkjet printing consisting of paper based flexible/wearable devices has a infinite potential into the coming generation devices, and other printed electronic application.

Chapter 1. Review of electrochemical energy storage devices.

1.1 Motivation

There are principally three types of energy sources in the world, such as fossil fuels, renewables, nuclear, and etc. Among them, 80.6% of energy consumption comes from fossil fuels, 16.7% from renewable resources look like biomass heat, solar power, hydropower, and nature wind, 2.7% from nuclear fission[1]. Human being is an outstanding evolution due to the industrial revolution in the meanwhile the consumption of the fossil fuels has been grown and undergoes serious problems such as depletion and greenhouse effect[2]. In order to solve these problems, demand is growing on energy sources that can be alternate fossil fuels: renewable and sustainable. In the case of renewable energy sources, the resources are affected by the weather and location. When it is cloudy and raining, the solar energy could not generate and in order to build the wind generation plant requires the strong wind and fat away from the city due to noise problems. Recently, energy storage systems have been taken attention for green energy source because it does not affect by the regions and weather condition and could use wherever we want to use electivity[3].

Consequently, the search for the next generation of energy-storage materials and devices such as rechargeable batteries and supercapacitors with pollution free operation, high efficiency, and a long cycling life is extremely important. Lithium ion battery(LIBs) has been mainly used in the world because it has high energy density. However, the battery suffers problems in low power density, which limits the application of battery in electric vehicles and hybrid vehicles requiring strong power and a long-term cycle property. Another spotlighted energy-storage system is supercapacitor due to strong power density and permanent usages, long term cycle life (> 100,000 cycles). Supercapacitors obtain a few hundred times higher power density than LIBs which are still higher energy density than conventional capacitors[4] . As illustrated in Figure 1.3, various energy storage devices are compared and presented in the Ragone plot. With the high-power ability than batteries and the relatively large energy density as compared to the conventional capacitors, and supercapacitors provide the enlarged potential devices to satisfy the growing power demands of energy storage systems(ESS). For these reasons, I will try to start the research about the supercapacitor.

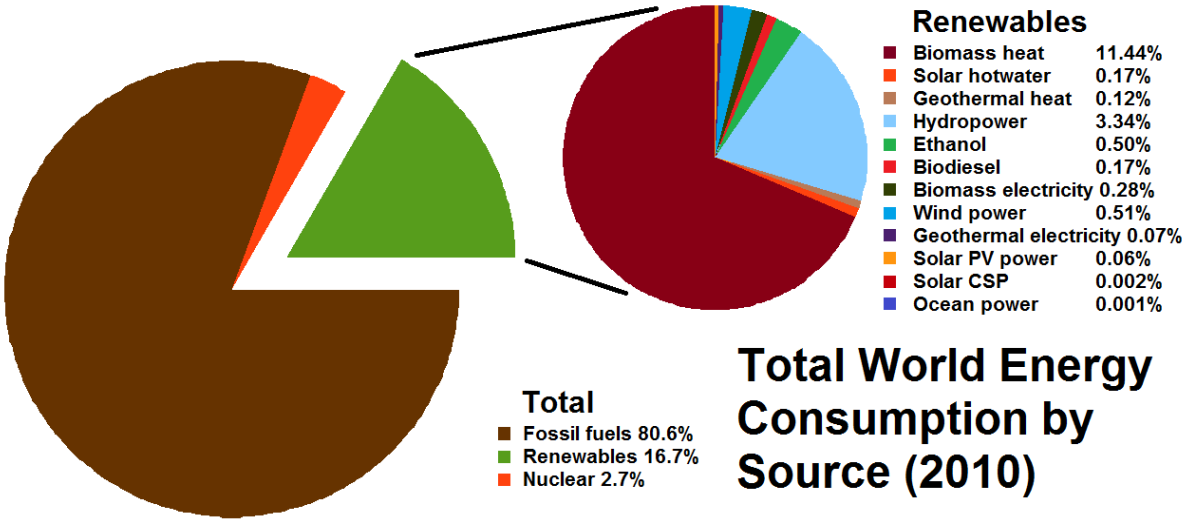

Figure 1. 1. Total world energy consumption by source (2010)[1]

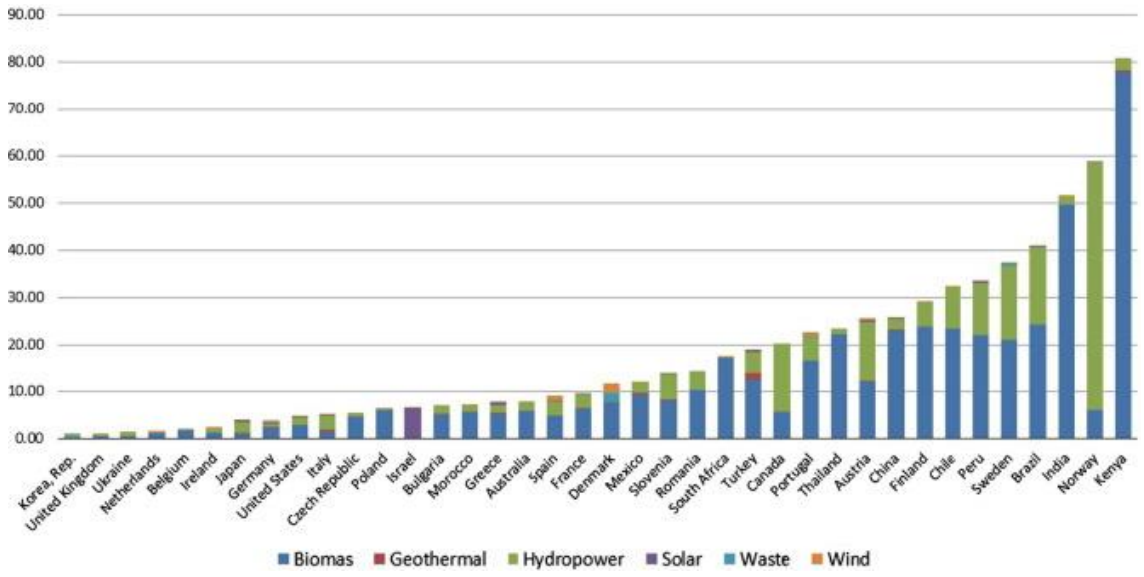

Figure 1. 2. The percentage of renewable energy sources in total final energy consumption: 1990-2010[2]

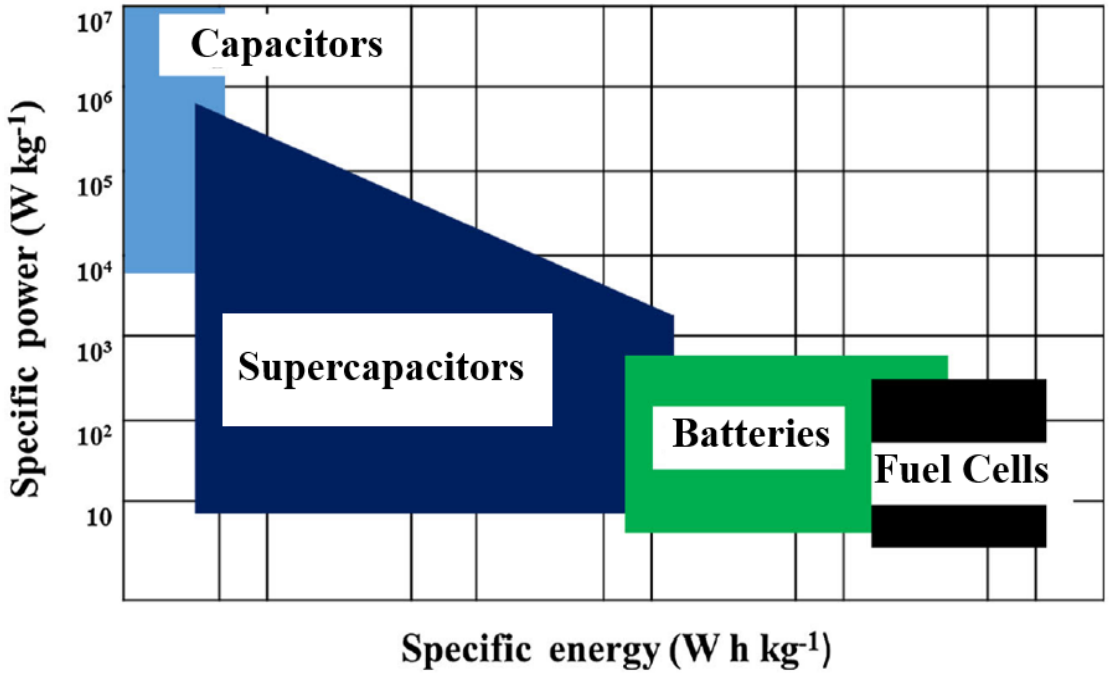

Figure 1. 3. Ragone plot of energy versus. power density for various ESS electronics.[3]

1.2 Supercapacitors

Supercapacitor consists of two electrode, positive and negative electrode, adding a current collector on each electrode at figure 1.4. Between the two electrodes, the separator was located, and electrolyte was full filled in the cells. As the power is applied on the electrodes, the positive electrode draws electrons / negative ions in the electrolytes and the negative electrode attracts cations. Finally, the charge separation happened on the electrode, and the charges stored on the surface of each electrode.

According to the mechanisms of energy storage at each electrode, the supercapacitors are distinguished in two kinds like Electric double layer capacitors (EDLC) and pseudo-capacitors. In case of EDLC, the charges are accumulated on the surface physically static forces, but the pseudo-capacitor stores the charges by chemically reversible redox reaction.

1.2.1 The mechanisms of energy storage

Conventional capacitors have lower capacitance and store only a few charges on the electrode. However, when porous materials as active materials are used, more than hundred times the charges are stored on the surface of the electrodes, which significantly improves the capacitance. Figure 1.5 schematizes the different models of EDLC mechanism and Figure 1.5a/b/c shows the Helmholtz[5], the Couy-chapman model[6,7] and Couy-Chapman-stern model[8], respectively[9]. Firstly, at Helmholtz model, the electrode draws the counter ions in electrolytes by making a monolayer on the electrode surfaces. The thickness of the thin monolayer is the approximate diameters of an ion in electrolytes. The Coup-Chapman demonstrates another type of model with considering the ion distribution in electrolyte solution. There is a diffuse layer and the ions could move in the electrolyte with concentration gradients. The Stern model combines the Helmholtz model with the Couy-chapman model and has two different layers. The inner region of thickness entitles a stern layer consisting of the inner Helmholtz plane (IHP) and the outer Helmholtz plane (OHP). The diffuse layer describes the Gouy-Chapman model. The capacitance of the EDLC is the combination of the capacitances of Stern layer (C_H) and Diffuse layer (C_{diff}), and then the total capacitance (C_{total}) can be expressed by the following equation:

$$\frac{1}{C_{total}} = \frac{1}{C_H} + \frac{1}{C_{diff}} \qquad (1.1)$$

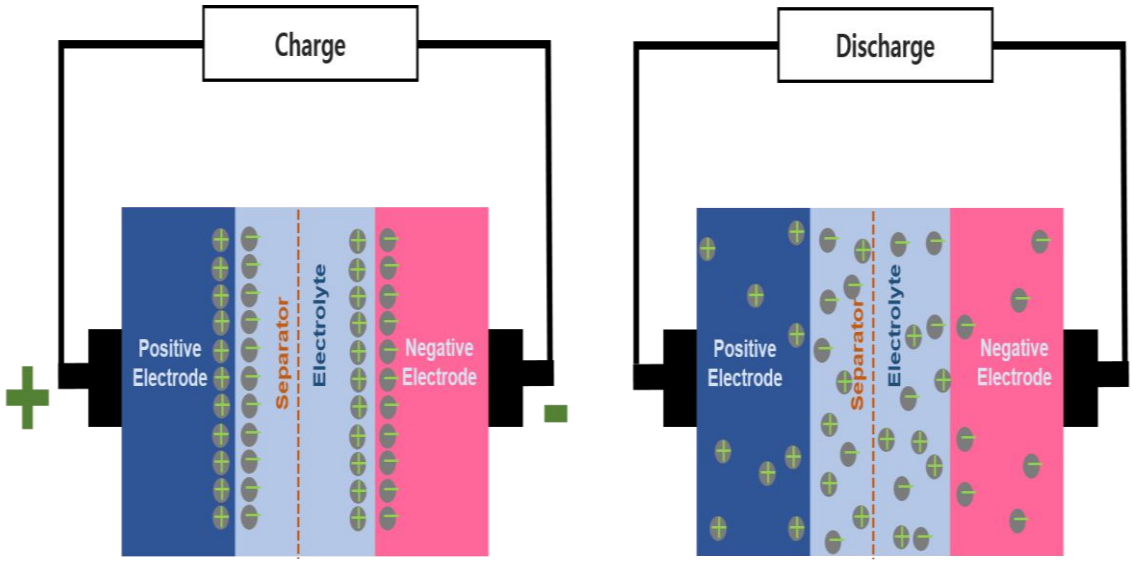

Figure 1. 4. Schematic of charge and discharge of the supercapacitors.

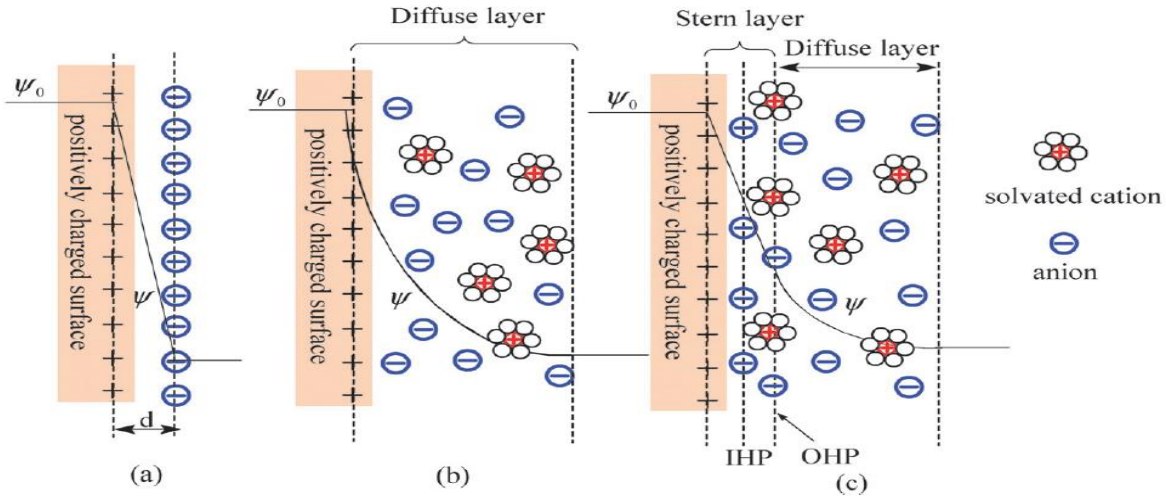

Figure 1.5. Models of electrical double layer surface: (a) the Helmholtz model, (b) the Gouy-Chapman model, and (c) the stern model, demonstrating the inner Helmholtz plane (IHP) and outer Helmholtz plane (OHP)[9]

1.2.2 The performance of the supercapacitors

EDLC have high power density and long cycle stability, but it has restriction to improve the capacitance because they only store the charges on the surface of the materials by electrostatic forces. To supplement the limitation of the EDLC, newly designed electrochemical capacitors are pseudo-capacitor. The word of pseudo-capacitance is from combining the prefix “pseudo” and ‘capacitance’ and Pseudo-capacitor stores the charges on the electrode surface by reversible redox reaction. The protons in electrolyte and charges in the electrodes are combined on the surface of the electrode and then the active materials are reduced[10]. From the mechanism, the capacitors accumulate the many charges on the surface of the electrode and Figure 1.6 show the distinct difference between EDLC and pseudo-capacitor. While the stored charges on the surface form a very thin layer on the surface in EDLC (Figure 1.6a) because EDLC could only operate from physical absorption, the pseudo-capacitors form the thick layer on the electrode surface by redox reaction(Figure 1.6b). Therefore, the pseudo-capacitors possess even higher capacitance than EDLC.

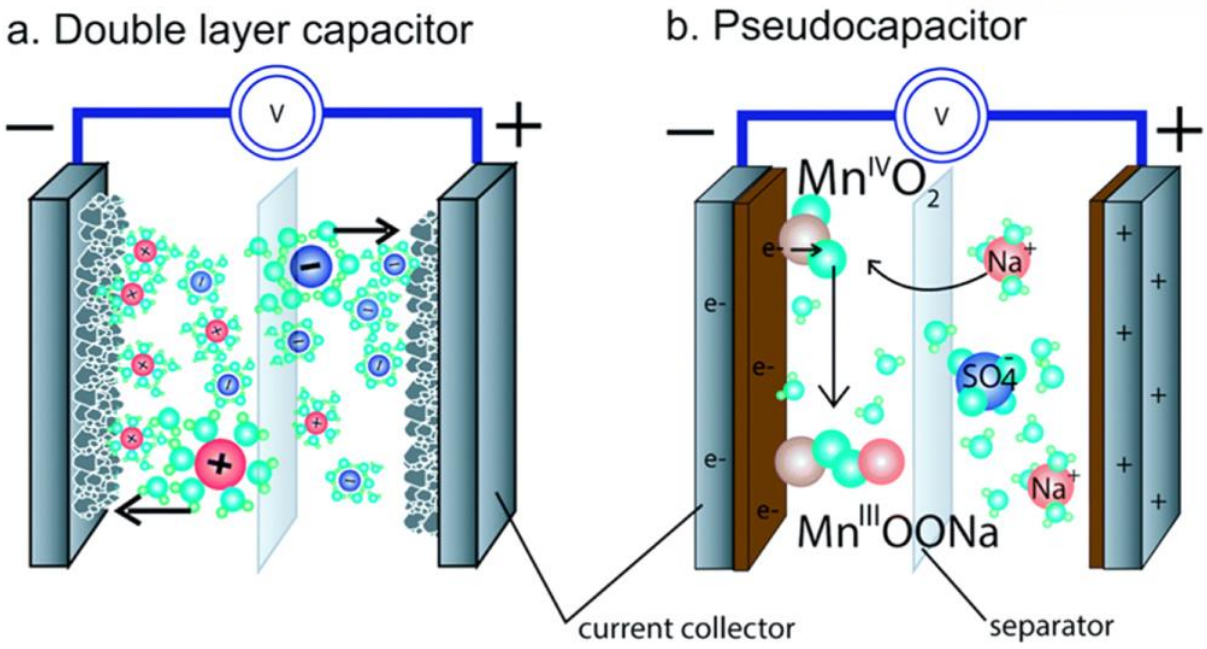

Figure 1. 6. Schematics of (a) all types of carbon materials for EDLC and (b) metal oxide/hydroxides for pseudo-capacitor, both devices have electrodes, a current collector, a separator and electrolyte

1.3 Electrode materials for supercapacitors

1.3.1 Carbon materials

Carbon based materials are used for the EDLC because they have high conductivity and large surface areas. There are many types of carbon materials including active carbons, nanotubes and graphene, carbon fibers, etc. Among carbon materials, active carbons are the mostly used as electrode materials due to their huge surface area, relatively outstanding electrical properties and appropriate cost. Kotz group[11] unveiled relation between surface area and capacitance. They discovered that the gravimetric capacitance is not proportional to the specific surface area, and capacitance showed similar value above 1200 m^2/g. The average pore thickness of the wall becomes close to the screening length of the electric field. Therefore, even though surface area is increased up to 1200 m^2/g, the pore thickness could no longer accommodate the equal amount of charge at a permitted electrode potential. In addition, larger percentage of bigger pores are more advantageous to improve the capacitance and fabricate the high-power supercapacitor because the larger size-pores can deliver high energy at high rate.

After the discovery of carbon nanotubes (CNT), many researchers extremely studied about CNT in electrical, optical, mechanical, and electrochemical properties due to their specific properties such as remarkable electrical properties, and good thermal and mechanical properties. The Single wall Carbon nanotubes (SWCNT) have a huge surface area about 1000 m^2 /g and show ohmic resistance less than 1Ω. Because of the good properties of the SWNT, the electrode based on the SWNT shows 69.4 Wh/kg of large energy density. Ion transportation in electrolyte solution plays a role as key factors to operate high energy density and high-power density[12,13].

Graphene is one of the carbon allotrope and is a structure in which carbon atoms are gathered to form a Two-Dimensionally (2D) plane. It is a one-atom-thick planar sheet that is densely packed with sp^2-boned carbon atoms, which forms a hexagonal lattice, called honeycomb structure[14,15]. In 2004, Graphene discovered by Andre Geim and Konstantin Novoselov at University of Manchester was attracted to many scientists[16,17]. Interest in graphene is due to the following outstanding characteristics. It has a high intrinsic carrier mobility of 200,000 $cm^2V^{-1}S^{-1}$ [18], a great thermal conductivity of 6000 $Wm^{-1}K^{-1}$ [19], an excellent mechanical property of 1.0 TPa and etc called Young's modulus[20].

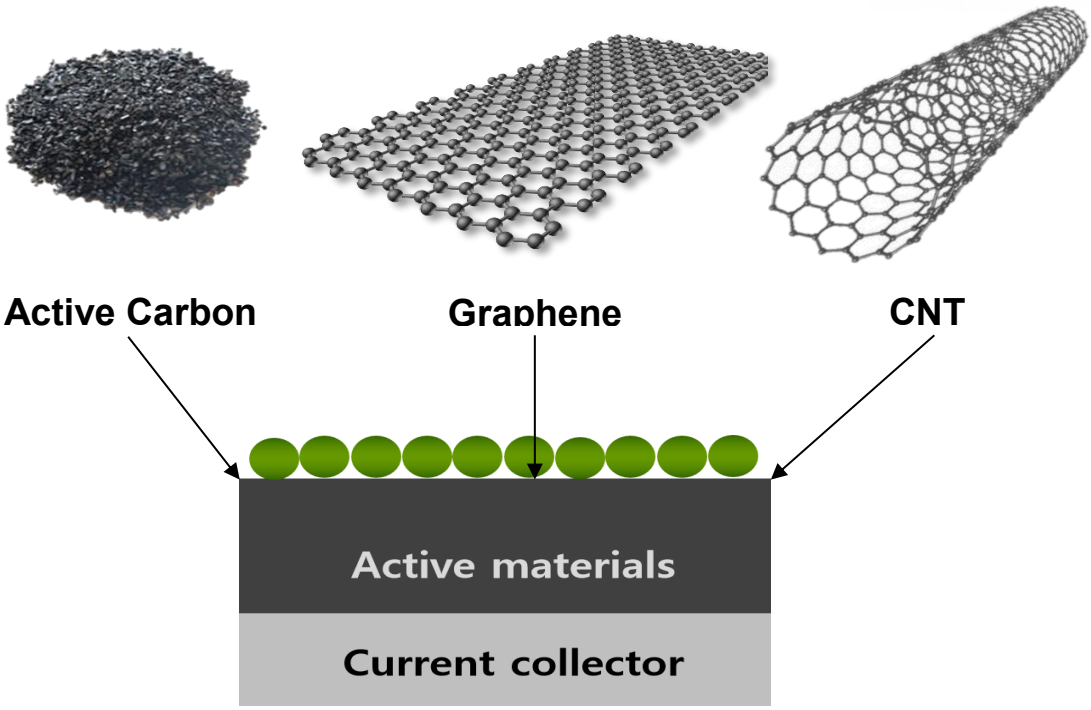

Figure 1. 7. Mainly used carbon materials for EDLC

1.3.2 Metal oxides

Metal oxides are the optimal candidate materials for pseudo-capacitor because they have larger energy density than EDLC based on carbon materials and good cycle stability than supercapacitor based on conducting polymer. Furthermore, metal oxides have about 10 to 100 times higher theoretical capacitance than EDLC as they store charges between electrode and ion in electrolyte by electrochemical faradic reaction. Between the metal oxides, RuO_2 is the most potential studied materials of the electrode due to its wide potential window, good theoretical capacitance, good proton conductivity, and long cycle life[21]. Even though RuO_2 have higher theoretical capacitance and higher conductivity than other metal oxides, RuO_2 have high cost and environmental harmfulness, which hinders the practical application[22]. For these reasons, researchers tried to find cheaper and environmentally friendly materials with similar electrochemical properties to RuO_2. Among many metal oxides, MnO_2, NiO, and $Ni(OH)_2$ take attention, because they provide low toxicity, low cost, environmental safety, also outstanding theoretical capacitances[23].

Zhitomirsky group reports MnO_x films and controls the thickness of MnO_x films by different deposition durations and then anneals the electrode at different condition because the crystallinity of MnO_x is changed to calcination temperature, which cause different electrochemical properties. When annealing the MnO_x at 300 °C, the crystallization of Mn_3O_4 phase is appeared, that of Mn_2O_3 is shown at 500 °C. The supercapacitor based on MnO_x films annealed at 300 °C indicated the specific capacitance of 445 F/g and the capacitance decreased by ~20% after 1000 cycles. Mn oxides also have several challenges like the low surface areas and low electronic conductivity and in order to address the problems, several approaches have been conducted[24].

$Ni(OH)_2$ is the bright materials as alternative electrode because it is not only low cost and eco-friendly but also has significant theoretical capacitance[25-27]. But it undergoes to low conductivity that researchers find difficulty in making higher theoretical capacitance of $Ni(OH)_2$ due to inferior rate capability and poor cycle stability less than 300 cycles[28,29].

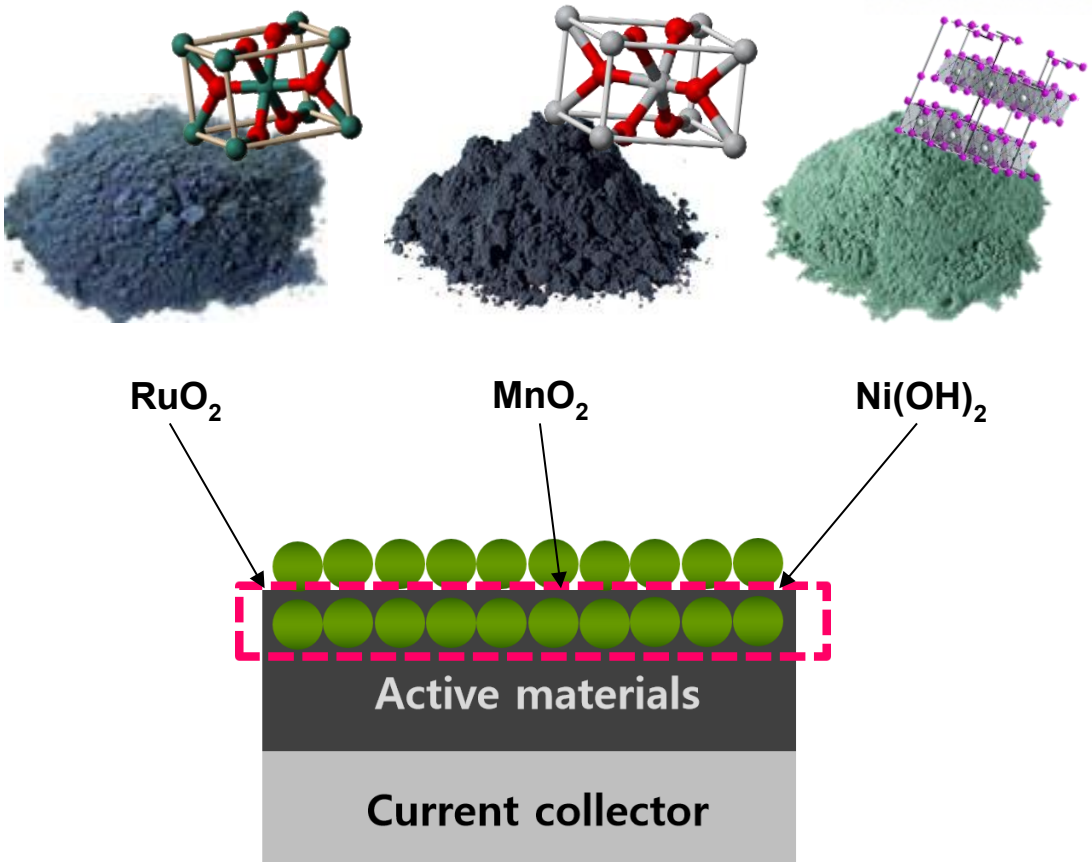

Figure 1.8. Various types of metal oxides for pseudo-capacitors

1.4 Reference

1. Martinot, E.; Sawin, J. L., Renewables 2012 global status report. *REN21 Renewable Energy Policy Network/Worldwatch Institute* 2012, *5*.

2. Laherrere, J., Forecasting future production from past discovery. *International Journal of Global Energy Issues* **2002,** *18* (2-4), 218-238.

3. Aleklett, K.; Campbell, C. J., The peak and decline of world oil and gas production. *Minerals and Energy-Raw Materials Report* **2003,** *18* (1), 5-20.

4. Winter, M.; Brodd, R. J., What are batteries, fuel cells, and supercapacitors? *Chemical reviews* **2004,** *104* (10), 4245-4270.

5. Helmholtz, H. V., Studien über electrische Grenzschichten. *Annalen der Physik* **1879,** *243* (7), 337-382.

6. Gouy, G., Sur la constitution de la charge electrique a la surface d'un electrolyte. *J. phys* **1910,** *9* (4), 457-468.

7. Chapman, D. L., LI. A contribution to the theory of electrocapillarity. *The London, Edinburgh, and Dublin philosophical magazine and journal of science* **1913,** *25* (148), 475-481.

8. Stern, O., Zur theorie der elektrolytischen doppelschicht. *Zeitschrift für Elektrochemie und angewandte physikalische Chemie* **1924,** *30* (21-22), 508-516.

9. Pilon, L.; Wang, H.; d'Entremont, A., Recent advances in continuum modeling of interfacial and transport phenomena in electric double layer capacitors. *Journal of The Electrochemical Society* **2015,** *162* (5), A5158-A5178.

10. Brousse, T.; Bélanger, D.; Long, J. W., To be or not to be pseudocapacitive? *Journal of The Electrochemical Society* **2015,** *162* (5), A5185-A5189.

11. Barbieri, O.; Hahn, M.; Herzog, A.; Kötz, R., Capacitance limits of high surface area activated carbons for double layer capacitors. *Carbon* **2005,** *43* (6), 1303-1310.

12. Niu, C.; Sichel, E. K.; Hoch, R.; Moy, D.; Tennent, H., High power electrochemical capacitors based on carbon nanotube electrodes. *Applied Physics Letters* **1997,** *70* (11), 1480-1482.

13. Futaba, D. N.; Hata, K.; Yamada, T.; Hiraoka, T.; Hayamizu, Y.; Kakudate, Y.; Tanaike, O.; Hatori, H.; Yumura, M.; Iijima, S., Shape-engineerable and highly densely packed single-walled carbon nanotubes and their application as super-capacitor electrodes. *Nature materials* **2006,** *5* (12), 987-994.

14. Chang, H.; Wu, H. Graphene-Based Nanomaterials: Synthesis, Properties, and Optical and Optoelectronic Applications. *Advanced Functional Materials* 2013, 23, 1984-1997.

15. Geim, A. K. Graphene : Staus and prospects. *Science* 2009, 324, 1530-1534.

16. Novoselov, K. S.; Geim, A. K.; Morozov, S. V.; Jiang, D.; Zhang, Y.; Dubonos, S. V.; Grigorieva, I. V.; Frirsov, A. A. Electric Field Effect in Atomically Thin Carbon films. *Science* 2004, 306, 666-669.

17. Soldano, C.; Mahmood, A.; Dujardin, E. Production, properties and potential of graphene. *Carbon* 2010, 48, 2127-2150.

18. Du, X.; Skachko, I.; Barker, A.; Andrei, E. Y. Approaching ballistic transport in suspended graphene. *Nat Nanotechnol* 2008, 3, 491-5.

19. Berber, S.; Kwon, Y.-K.; Tomanek, D. Unusually High Thermal Conductivity of Carbon Nanotubes. *Phys Rev Lett* 2000, 84, 4613-4616.

20. Zheng, Q.; Li, Z.; Yang, J. Effects of N doping and NH2grafting on the mechanical and wrinkling properties of graphene sheets. *RSC Adv.* 2013, 3, 923-929.

21. Kim, I.-H.; Kim, K.-B., Electrochemical characterization of hydrous ruthenium oxide thin-film electrodes for electrochemical capacitor applications. *Journal of The Electrochemical Society* **2006,** *153* (2), A383-A389.

22. Kim, Y.-T.; Tadai, K.; Mitani, T., Highly dispersed ruthenium oxide nanoparticles on carboxylated carbon nanotubes for supercapacitor electrode materials. *Journal of Materials Chemistry* **2005,** *15* (46), 4914-4921.

23. S.-I. Kim, S.-W. Kim, K. Jung, J.-B. Kim and J.-H. Jang, Ideal nanoporous gold based supercapacitors with theoretical capacitance and high energy/power density, Nano Energy, 2016, **24**, 17-24.

24. Nagarajan, N.; Humadi, H.; Zhitomirsky, I., Cathodic electrodeposition of MnO x films for electrochemical supercapacitors. *Electrochimica Acta* **2006,** *51* (15), 3039-3045.

25. Li, J. T.; Zhao, W.; Huang, F. Q.; Manivannan, A.; Wu, N. Q., Single-crystalline Ni(OH)(2) and NiO nanoplatelet arrays as supercapacitor electrodes. *Nanoscale* **2011,** *3* (12), 5103-5109.

26. Patil, U. M.; Gurav, K. V.; Fulari, V. J.; Lokhande, C. D.; Joo, O. S., Characterization of honeycomb-like "beta-Ni(OH)(2)" thin films synthesized by chemical bath deposition method and their supercapacitor application. *J Power Sources* **2009,** *188* (1), 338-342.

27. Lu, Z. Y.; Chang, Z.; Zhu, W.; Sun, X. M., Beta-phased Ni(OH)(2) nanowall film with reversible capacitance higher than theoretical Faradic capacitance. *Chem Commun* **2011,** *47* (34), 9651-9653.

28. Yang, G. W.; Xu, C. L.; Li, H. L., Electrodeposited nickel hydroxide on nickel foam with ultrahigh capacitance. *Chem Commun* **2008,** (48), 6537-6539.

29. Zhong, J. H.; Wang, A. L.; Li, G. R.; Wang, J. W.; Ou, Y. N.; Tong, Y. X., Co3O4/Ni(OH)(2) composite mesoporous nanosheet networks as a promising electrode for supercapacitor applications. *J Mater Chem* **2012,** *22* (12), 5656-5665.

Chapter 2. Printable asymmetric supercapacitors using Interconnected 3D graphene

2.1 Introduction

Wearable electronics are growing in market due to their seamless transition in everyday human life interaction. These devices could be attached onto anywhere, which can be directly attached onto human skin for application such as implantable medical devices, environmental monitoring sensors and self-power supply[1-3]. In addition, they can be sustained by exploiting things in Radio Frequency Identification (RFID), Machine to Machine (M2M), Ubiquitous Sensor Network (USN), and so on. To activate these devices, these devices are needed to be have numerous conditions such as easy access, flexibility, low-cost, scalable manufacturing, environmentally safe, high performance, and so forth. Many researchers feel interest in supercapacitor, which have been widely researched over these days because of their excellent power density, operational cycle time, rapid charge-discharge rate, environment-free operation and facile manufacture[4-6]. Therefore, supercapacitors are suitable device because it can manufacture electrode by using various techniques, such as inkjet printing, 3D printing, spray-coating, electrodeposition, photolithography, sputtering and, etc[7-10].

Of those, inkjet printing is useful that immediately can be applicable technique in this rapidly changing electronics market. Besides, through these processes, fabricated electrodes are facile, cost effective, scalable, and compatible to the current market, compare to expensive laser instrument, multi-step photolithography and other printing methods[11,12]. Inkjet printing electrodes using desktop printer (HP Officejet Pro 8100) could be controlled by the number of printing, size of designed patterns and letters (interdigital patterns, maps and, etc.) and could be exactly integrated with each anode/cathode. However, it is most important to consider the conducting inks of rheological properties (Fromm number, Z), which are regulated from the surface tension, liquid density, viscosity and particle size in order not to clog the head of cartridge[13-16].

Solid-state supercapacitors having flexibility have recently obtained remarkable interest that previously studied different substrate including polymer film, textile, thin glass, membrane and paper[17-20]. A4 Paper is the most appropriate choice to print using commercial desktop printer and has a few advantages (moderate prices, eco-friendly, outstanding flexible, light-weight). In the most of cases, carbon materials that store charges on electrical double layers(EDL), such as activated carbon, various type of graphene oxide, porous carbon, carbon nanotube (CNT), were studied in these field. In contrast

to EDL, pseudocapacitive materials, including RuO_2, MnO_2 and conducting polymer, are faradic reaction, including rapid / reversible redox reactions between electrolyte and electrode covered active materials[21,22]. Carbon materials have excellent stability but relatively low capacitance, transition-metal oxides that has larger than EDLC values surfer from the disadvantages due to poor electrical conductivity, surface area, dissolution in electrolytes, narrow potential window and low cycle stability. This challenge could be solved through fabricating an asymmetric supercapacitors (ASCs), which composed to different materials as positive and negative electrodes[23,24].

Recently, various types of carbon-based materials are used mainly as electrode materials because of having their high conductivity, chemical stability, and a huge surface area for energy storage devices. Owing to mentioned remarkable advantages of graphene, numerous scientists have been interested in the study of its various applications. Despite the excellent performance of 2D materials in many applications, there are two problems that the graphene layers have restacked onto each other and the pores as active sites are lacking[25,26]. Because of the resistance to mass transfer increase, and the active sites becoming clogged, it leads to poor electro-catalytic performances. To solve these drawbacks, Three-Dimensional Graphene Nano-networks (3DGNs) are great solution containing micro- (<2nm), meso- (2-50nm), and macro-sized (>50nm). Thanks to these pores, mass transfer can be accelerated that have a tremendous surface area and provide many active sites as well as channels.

Herein, we study the synthesis of 3DGNs[27,28], which have different shapes and mass production using various template such as globular polymer and wood. 3DGNs are synthesized by CVD process using a spherical polymer template penetrated PVA/metal precursor solution. Here, the polymer or wood serve not only as a carbon source, but also as a template-making structure, and the metal precursor acts as a catalytic material to grow graphene. Through the etching procedures, 3DGNs has a high surface area (961 m^2 / g) due to the removal of metal particles, formed a number of micro/meso-pores. And a high-quality 3D graphene has been synthesized due to the appropriate amount carbon sources and metal precursor in CVD. With these materials, we have confirmed an excellent specific capacitance of 355 F/g and well retention after many life times at EDLC. Because of both a bulk surface area and high-quality graphene properties, synthesized 3DGNs are expected to be applicable in a wide of areas such as 3D electrodes and ESS.

In this chapter, with this printing technology, we can easily adjust the shape and size of electrode on the paper substrate and simply attach to things (wall as wallpaper, sensors, and etc.) to realize IoT. Using printed electrodes instead of wallpaper can compensate for esthetic parts of IoT devices that are connected by electric wires and is lighter and more efficient than conventional coin cell. We demonstrated the facile printable asymmetric supercapacitors (PASs) using commercial desktop inkjet

printer by fabricating ASCs on A4 paper-substrate. Because A4 paper has very poor electrical property, firstly, CNT inks that have electrical and mechanical properties were printed on paper-substrate as current collector in magenta cartridge. Herein the novelty in this study is that it is possible to produce high efficient supercapacitors using carbon materials without using expensive metals such as Au, Ag, etc. Next, we that use diverse patterned printing for demonstration exploit i-3DGNs inks for the negative materials and added MnO_2 inks for the positive materials, respectively black and yellow cartridge. Since dispersing agent is an insulator, the inkjet-printed materials have to be washed immediately to remove dispersion agent and dry. To assemble PASs, aqueous gel electrolyte was loaded on the electrodes and fully dried samples were packed by PET films. We identify the fabrication of conducting form by desktop printer. Following that PASs are fabricated by assembling the electrode inks, it shows a broad operating potential window of 1.8 to 2.0 V and exceptional electrochemical performances, which is the areal, volumetric capacitance and cycle stability represented in these devices.

2.2 Experimental section

2.2.1 Materials

Methyl methacrylate (MMA), methacrylic acid (MA), polyvinyl alcohol (PVA, 31,000~50,000/ 89,000~98,000 of molecule weight), Lithium Chlororide (LiCl), polyvinylidene fluoride (PVDF), 2,2'-azobis(2-methylpropionamidine) dihydrochloride (AAPH), Isopropyl alcohol (IPA) and sodium dodecylbenzene sulfonate (SDBS) were purchased from Sigma-Aldrich. N-Methyl-2-Pyrrolidone (NMP), potassium hydroxide and was purchased from Samchun chemicals. Nickel chloride hexahydrate was purchased by YAKURI Pure chemicals. Poly(elethylenimine) (PEI) was purchased from Junsei Chemical Co. Ltd. SWCNT power and solution was obtained from Tubal™, OCSIAL / KH chemicals Co. Ltd, respectively.

2.2.2 Preparation of various polymer template

Firstly, Poly(methyl methacrylate) , PMMA spheres are prepared from an emulsion polymerization method. The synthesis of polymer spheres is accomplished as follows. Methyl methacrylate (50mL), 2,2'-Azobis(2-methylpropionamidine) dihydrochloride(1.45mmol) as initiator and Milli-Q water (400mL) were progressed into a 500mL RB flask equipped with a magnetic stirring device, and temperature controller at nitrogen atmosphere. After pursing, the temperature is controlled up to 50°C. The reaction is allowed to proceed for 2hr and polymer spheres (300nm) are obtained as a stable dispersion in water[29,30].

Because PMMA is a hydrophobic polymer, it is a drawback that it does not mix well with a metal precursor solution. So, by adding methacrylic acid (MA) to make a copolymer, these disadvantages are compensated. Poly(methyl methacrylate-co-methacrylic acid), Poly(MMA-co-MA) spheres are also made by an emulsion polymerization.

These spherical copolymers can be synthesized in various sizes (300nm ~ 1.4um) depending on reaction time, temperature and amount of components such as monomer, initiator, and dispersion media. In the process of the polymerization, firstly, polymer nuclei are rapidly produced in emulsion solution. As the reaction time increased, unstable polymer seeds are grown through the swelling process of copolymer and the monomer concentration in the process become lower and lower. When the monomers are exhausted, the growth of the particles eventually stops. Because of these reasons, the amount of each components is very important to control of the polymer particle size.

As another method for making hydrophilic PMMA, there is a method of wrapping a hydrophilic linear polymer. The PEI is a high viscosity and water-soluble polymer. When PMMA polymer is mixed with PEI dissolved in water, a relatively hydrophilic polymer template can be obtained. Also, Because PEI is a polymer with repeating unit included of the amine group, there is an advantage that nitrogen can be doped in 3DGNs for improved conductivity at carbonization. .

2.2.3 Synthesis of 3DGNs

PVA solution as carbon source (2wt% of solvent) completely dissolved in DI water at 85ºC, which is mixed in $NiCl_2 \cdot H_2O$ (300wt% of carbon source) as catalyst for a several minutes. Figure 2.1. show that the polymer templates (8wt% of solvent) put into this solution and stirred until completely dispersion of template and precursor solution[31,32]. And then the dispersed solution dried in vacuum oven to evaporate water. The dried mixture is placed in quartz tube (Scientech Corp.), heated to 1000ºC under Ar (200 sccm)/H_2 (100 sccm) atmosphere, subsequently located in isothermal conditions for only 30 min. After heating, the reacted samples immediately are cooled at room temperature for crystalline. Synthesized 3DGNs samples are immersed on HCl (10 vol%) during 24hr for removal of Nickel and we could obtain High porosity and well electrical conductivity samples[27].

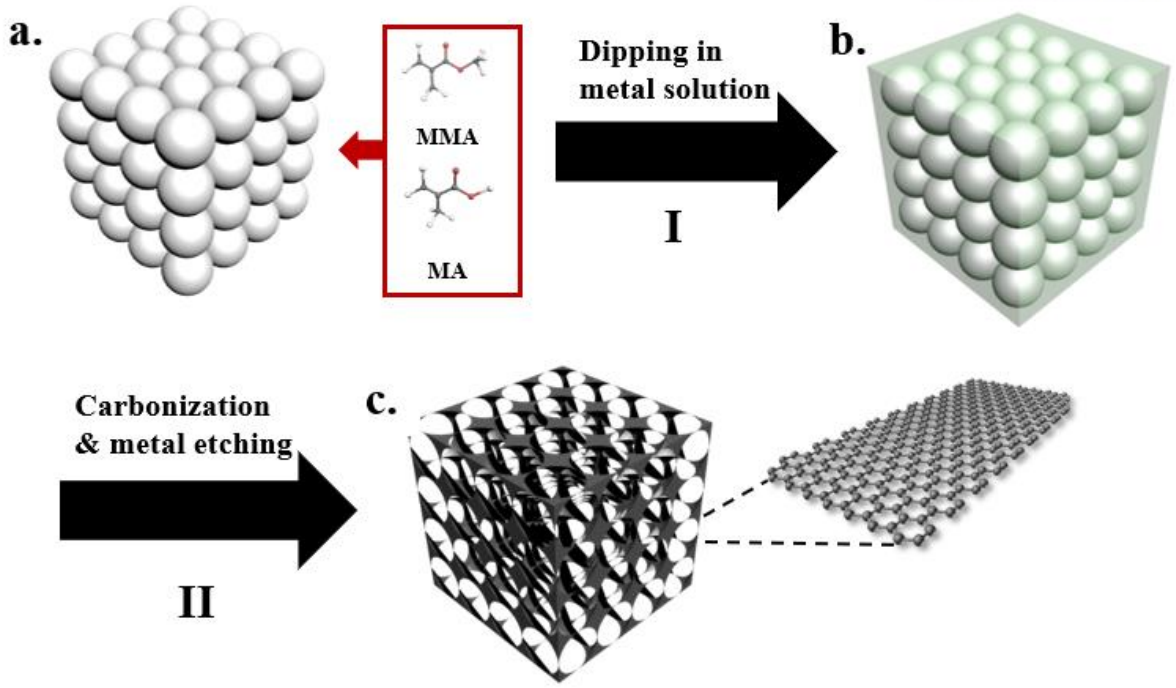

Figure 2.1. Schematic illustration of synthesis process for 3DGNs, (a) template of polymer through emulsion polymerization, (b) Immersed template in PVA/metal solution, (c) Through carbonization, synthesized 3DGNs in CVD and residue of metal etching.

2.2.4 Fabrication of interconnected 3DGNs / adding MnO_2 inks using each electrode

For the negative electrode, the interconnected 3DGNs (i-3DGNs) inks are prepared by ultrasonication for 60min, which contain 3DGNs powders, SWCNT powder (5wt% of 3DGNs) as Interconnector and SDBS as surfactant in IPA solution. For the positive inks, the i-3DGNs inks added MnO_2 powder are sonicated to fabricate a stable ink and is also supplement SDBS because appears some precipitation. For the MnO_2 nanoparticles are synthesized by following method. $KMnO_4$ is dissolved in DI water, and then Ethanol added led to formation of brownish precipitated MnO_2. Reduced mixtures are stirred for 24hr and then the precipitates are filtered, washed with DI water / EtOH to eliminate the by product and non-reaction product and dried at the oven[33]. The physical properties of different inks are optimized to meet requirement of the printing inks, and the inks are infused to clean ink cartridge. To solve clogging of the cartridge head, each electrode for inks in IPA is subjected to centrifugation (at 3000rpm for 1 h) to remove large-sized particles and agglomerates before Being filled into the cartridge. The inks are injected into each colored cartridge, black – negative materials / yellow – positive materials / magenta – SWCNT acting as current collector.

2.2.5 Fabrication of printable asymmetric supercapacitors using each ink

A HP Officejet Pro 8100 printer is exploited current collector, negative and positive electrode materials on a A4 paper. When we perform to print the PAS electrode, the print setting configures the high-quality mode that prints the large amount of ink on the A4 substrate. To fabricate the electrodes for PASs, magenta color filled into SWCNT solution is firstly printed to deposit a several layers of SWCNT playing a role of current collector on the substrate, and then wet state electrodes are completely dried. On the SWCNT film, black or yellow inks are printed to fabricate several electrode layers, which each ink separately print to act as negative or positive electrode. To attain various images of PASs electrode on the substrate, the programs such as the photoshop or CAD could be used to design the printed letters or patterns. Also, this method could be quickly and simply patterned and performed versatile shapes and size printing. The solid-state PAS is gathered by using PVA-LiCl gel electrolyte as separator at the same time. For the fabrication of the gel polymer electrolyte, PVA having 89,000~98,000 of molecule weights is clearly dissolved in DI water at 85^{o}C for 2h with vigorous stirring, and LiCl are subsequently mixed in PVA solution. The as-prepared gel electrolyte is plastered on each electrode and solidified within 24hr at 45^{o}C oven. PAS device is packed with PET tape to prevent moisture absorption in the gel electrolyte[34].

2.2.6 Materials and electrochemical characterization

The morphologies of the as-prepared samples were characterized using SEM (Nano230 FE-SEM) and TEM (normal TEM, JEM-2100). The crystallinity was measured by using XRD (X-ray diffraction measurements, High power XRD, from 10 to 70). To confirm the structure and bonding between components of samples were characterized by Raman spectroscopy (WITec, alpha300R, 532nm Lazer) and XPS (X-ray Photoelectron Spectroscopy, Thermo Fisher Scientific, ESCALAB 250XI). The surface area, pore size, and pore volume were carried out using the BET (Brunauer-Emmett-Teller, Belsorp max, Bel Japan). The sheet resistance of printable sample was measured by 4 point-probe (Dasol Eng, FPP-RS8, pin-spacing 1mm, pin-radius 100um). The ink viscosities were measured by a rheometer (Kinexus, Malvern,).

Electrochemical performances for supercapacitor were checked both in a three-electro system. The supercapacitor properties of a positive electrode and a negative electrode were evaluated using Platinum mesh, Ag/AgCl electrode, and various electrolyte (1M H_2SO_4, 6M LiCl) as counter electrode, reference electrode, electrolyte, respectively. All electrochemical tests including cyclic voltammetry (CV), galvanostatic charge/discharge (GCD), and electrochemical impedance spectroscopy (EIS) were performed by electrochemical workstations (VMP3 biologic electrochemical workstation and Versa STAT 3, AMEKTEK). Further, an asymmetric printable supercapacitor using inter-connected 3DGN (negative) and adding MnO_2 (positive) were tested in a two-electrode configuration using PVA-LiCl gel polymer electrolyte.

The gravimetric, volumetric and areal capacitance of PASs were estimated from the cyclic voltammetry and galvanostatic charge/discharge profiles using the following equations:

Cyclic Voltammetry:

Capacitance: $$C = \frac{\int i dV}{2S\Delta V} \quad (1)$$

Galvanostatic charge/discharge:

Capacitance: $$C = \frac{I \times \Delta t}{\Delta V} \quad (2)$$

Gravimetric capacitance: $$C_g = \frac{C}{m} \quad (3)$$

Volumetric capacitance: $$C_v = \frac{C}{v} \quad (4)$$

Areal capacitance: $$C_a = \frac{C}{a} \quad (5)$$

Where C is the capacitance (F), C_g is the gravimetric capacitance (F g^{-1}), C_v is the volumetric capacitance (F cm^{-3}), C_a is the areal capacitance (F cm^{-2}), S is the sweep rate (mV s^{-1}), $\triangle V$ is the potential window (V), I is the discharge current (A), $\triangle t$ is the discharge time (s), v is the volume of the electrode material (cm^3), m is the mass of the active material (g), A is the area of the electroactive material (cm^2), l is the length of the electrode material and $\int i dV$ is the integral area of the CV curve (A).

At the PASs, the stored electric charge of positive electrode to negative electrode was calculated by the following equation:

$$m_+/m_- = V_- C_-/V_+ C_+ \quad (6)$$

where m is the mass loading of electroactive materials, V is the potential window and C represents the specific capacitance, respectively.

2.3 **Results and Discussion**

The fabrication of the 3DGNs is shown in Figure 1.9. a) as-prepared the Poly(methyl methacrylate-co-methacrylic acid) P(MMA-co-MA) were soaked in the aqueous Ni precursor. Because carboxyl group of methacrylic acid offer the wettability, Ni solution could penetrate evenly between polymers. After complete drying via oven, yellowish green powder (Figure 1.9. b) was made in a form that is well wrapped in polymer sphere. The Ni precursor / polymer mixtures are carbonized through CVD procedure under the H_2 / Ar atmosphere. To obtain a good-quality of 3DGN that allowed for high electrical conductivity and we optimized condition which adjusted ramping rate of temperature, reaction time and flow of the gas. Since the temperature at which P(MMA-co-MA) is decomposed is about 400^{o}C, it is difficult to maintain a spherical shape of 3DGNs at high temperature in the range of 800-1000 ^{o}C. So, at isothermal conditions of 1000 ^{o}C, the dried mixture synthesized for only 30 min. After heating, the samples immediately are cooled at room temperature for crystalline. The quenching process could prevent changes in the inside of 3DGN and metal particles and provided inverse opal structures. During heat process in CVD, nickel precursors are reduced into nickel particles that catalyzed the growing of graphene as a metal catalyst, and aggregated Ni particles formed pores from 1 nm to 100 nm on the 3DGN surface. Through these process, the sample of 3DGNs has the macro, meso, micro-pores, which are appropriated for both high rate performance and high-density energy storage[35] at the same time.

A scanning electron microscopy (SEM) of P(MMA-co-MA) and 3DGNs and transmission electron microscopy (TEM) of 3DGNs (Figure 1.10. a, b, c) shows each specific shape with spherical and inverse opal structures. The nanoporous structures with high surface area with ample active site over hierarchical pores can improve the mass transport by reducing the resistance of diffusion as well as supply ion transport, which are critical in developing outstanding capacitance electrodes[36,37].

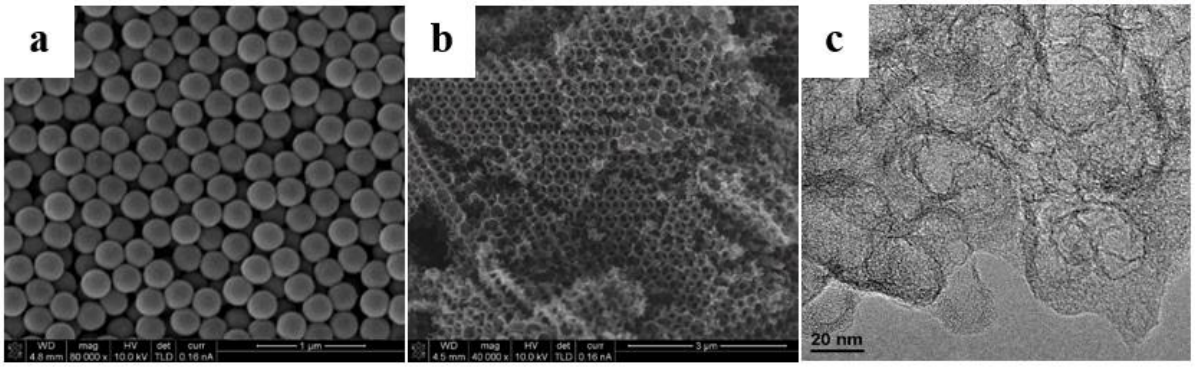

Figure 2.2. Morphology characterizations of 3DGNs (a) SEM image of spherical polymer. (b) SEM image of 3DGNs using polymer template as carbon sources under Ni precursor and TEM image (c).

The measurement of X-ray diffraction (XRD) are analyzed to verify the removal of Ni (111) peak, which appears at 44.5° at Figure 1.11 a). Compared to the data from the original graphene having strong and shape peak, 3DGNs have one broad peak represented the (002) plane of the graphene. This XRD peak proves that the Ni particles are absolutely removed to the almost single crystalline, which shows the ability of completely created single crystalline at 25° [37] .

Raman sprectroscopy of the 3DGNs demonstrates the graphitic property with G-peak located at 1581 cm^{-1} , D-peak at 1341 cm^{-1} / 2D-peak at 2700 cm^{-1} related to the stretching of sp^2-bonded pairs, the sp^3 defected sites at Figure 1.11 b), respectively[38]. X-ray photoelectron spectroscopy are indicated to analyze the element consist of the 3DGNs at Figure 1.11 c, d. Figure 1.11 c) shows the C1s spectra, which are indicated that the crucial fraction of carbon is sp^2 C at 284.6 eV, followed by sp^3 hybridized C at 285.3 eV along with minor contribution from different bonding configuration of carbon with oxygen. The O 1s spectra demonstrates a presence of oxygen fuctional groups such as C-OH, C-O at 532.6 eV [39] .

The porous structure of 3DGNs is analyzed by N_2 adsorption/desorption isotherms, which shows a plot with a fast increase at a high pressure indicating that the pore volume is mostly to mesopores[40]. The Barret-Emmett-Teller (BET) surface area of 3DGNs is 961 m^2 / g. Because of the generation of pores from of many volatile gases during CVD process and removal of the metal paricle, 3DGNs have the increased surface area[41]. The average diameter value of mesopores from the Barrett-Joyner-Halenda (BJH) is 11.81 nm for 3DGNs derived P(MMA-co-MA), which is signified that the porosity could be controllable by using the various sized polymers even the same process is tried.

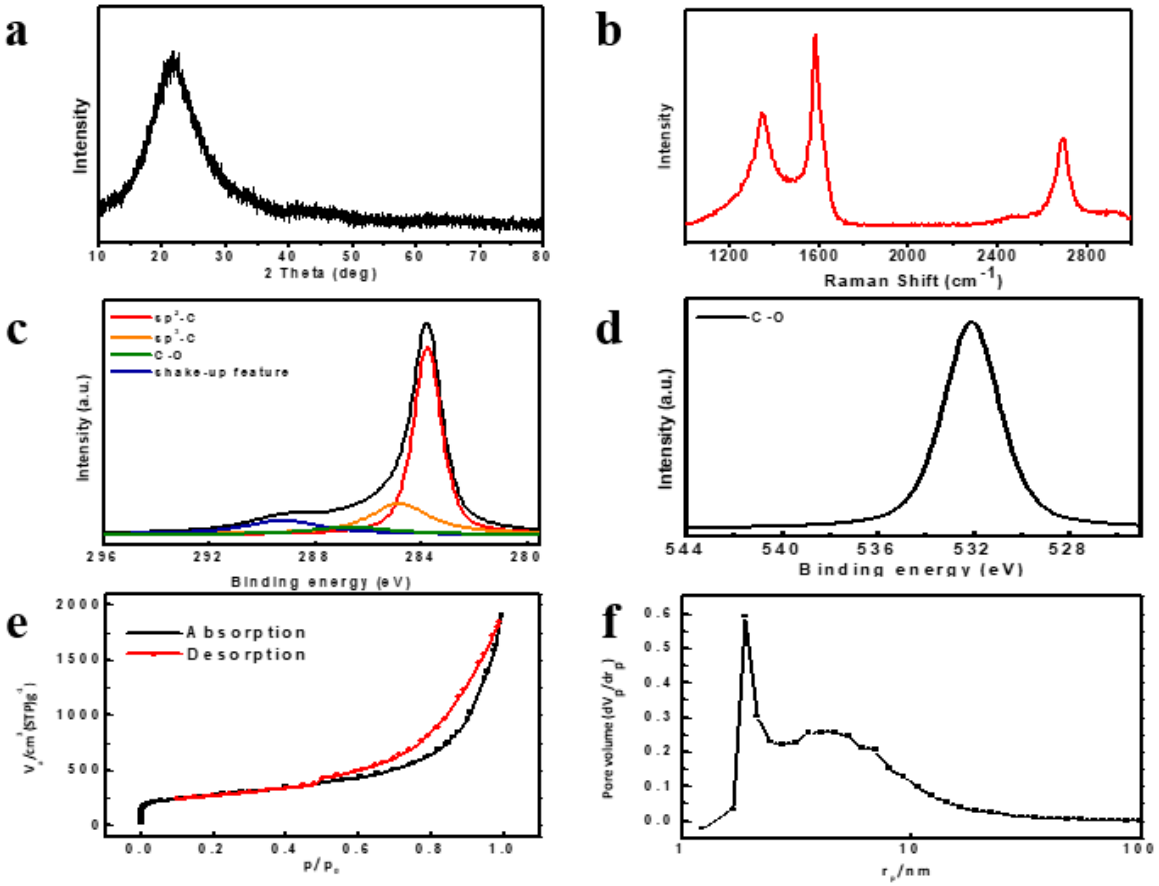

Figure 2.3. Characterization of 3DGN electrode. (a) XRD data, (b) Raman spectra, (c-d) XPS. (e) N_2 adsorption/desorption isotherms plot and (f) pore size distribution graph of 3DGNs.

The electrochemical properties of 3DGNs electrode are analyzed by cyclic voltammetry (CV), galvanostatic charge-discharge (GCD) as EDLC electrode. Here we use a 3DGNs with high surface area of 961 m^2/g fabricated on a mass production. Figure 2.4 a) shows the CV of three electrodes assembly with 3DGNs as the active material at a wide range of -0.2 V to 0.8 V vs Ag/AgCl. Overall, at the supercapacitors that use carbon-based electrode, the CV curve and the capacitance can be considerably degrade when the voltage scan rate increases, representing distortion of the rectangular shape. The CV curves of 3DGNs supercapacitor at all scan rates besides the highest scan rate of 100 mV/s are almost rectangle shape, showing that 3DGNs are an ideal carbon electrode material with excellent capacitance. A significant specific capacitance of 315 F/g in 1M H_2SO_4 solution is obtained at a current density of 2 A/g, calculated by equation (1).

However, unlike previous studied 3D-GN in our group that are synthesized from a silica-based template, these 3DGNs samples is fabricated on a less rigid template from polymer, resulting in a large loss of the capacitance about 39% from 2 A/g to 20 A/g. To compensated for this problem, we last our research on improving the conductivity, cycle stability and performance of 3DGNs by adding single wall carbon nanotube (SWCNT), which could serve as bridge, it is called interconnected 3DGNs (i-3DGNs). When i-3DGNs contain too much SWCNT, it blocks the pores of 3DGNs, so that 5wt % of SWCNT could provide appropriately larger surface area and at the same time as the optimized interconnected samples.

Figure 2.5 show that each SWCNT between 3DGNs are well connected and serve as a linker from SEM and TEM images and c, d) indicate Raman spectra of SWCNT, 3DGNs and i-3DGNs. Radical breathing mode (RBM) corresponds to radial expansion-contraction of the CNT. Therefore, its frequency V_{RBM} depends on the diameter of CNT as $V_{RBM} = A/d + B$ and can be estimated, which is very useful in deducing the diameter of CNT from the RBM position. Because RBM range is typically 100~350 cm^{-1},The Figure 2.5. d) signify interconnected samples at RBM of i-3DGNs about 200 cm^{-1} [42,43].

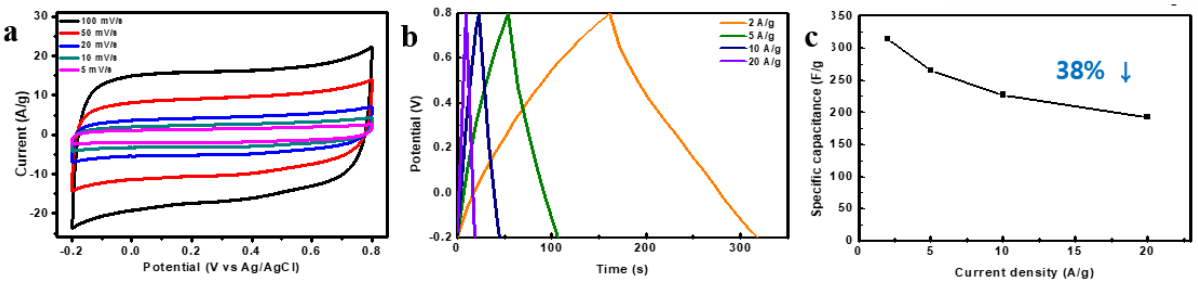

Figure 2.4. Electrochemical performance of 3DGNs supercapacitors. (a) Cyclic voltammetry curves of 3DNGs electrode at the scan rate of 5 to 100 mV/s. (b) Galvanostatic charge-discharge plots of 3DGNS at a current density of 2 A/g to 20 A/g. (c) Specific capacitance values as a variety of current density. (d) Nyquist plot of 3DGNs electrode in 1M H_2SO_4 electrolyte solution compared to Activated carbon.

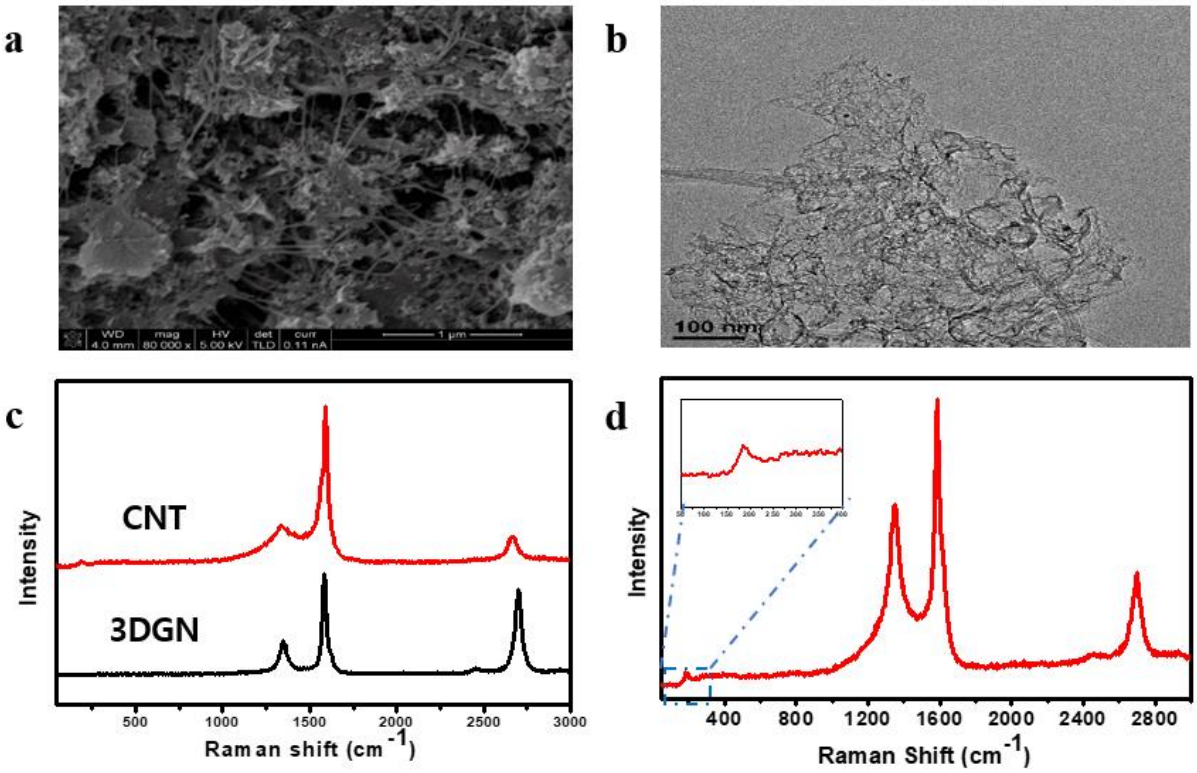

Figure 2.5. Morphology characterizations of i-3DGNs (a) SEM and (b) TEM images. The Raman spectroscopy of each samples. (c) SWCNT and 3DGNs. (d) the RBM of i-3DGNs including 5wt% SWCNT with 3DGNs.

i-3DGNs electrodes are also measured by the same methods such as CV, GCD as EDLC electode. the measurement of electrochemical property included CV, GCD, cycle stability and electrochemical impedance spectroscopy (EIS) confirmed that i-3DGNs electrodes have better performance than 3DGNs electrodes in 1M H_2SO_4. The CV curves of i-3DGNs electrodes at a scan rate from 5 to 100 mV/s are shown in Figure 2.6. a). These curves clearly exhibit the typical rectangular shape demonstrating the ideal capacitive behavior and excellent electrochemical performance of i-3DGNs electrodes, which have broader integration area compared to 3DGNs. When the scan rate increases, the ions included in the electrolyte solution quickly shift from the bulk electrolyte to the electrode/electrolyte interface. However, the electrochemical adsorption and desorption of electrode materials at parts of the electrode materials don't be performed well due to the relatively slow diffusion rate of ion from electrode/electrolyte interface to the inner electrode materials. Therefore, most of the ions are accumulated by the electrode/electrolyte interfacing and polarized on electrode materials.

The effect of interconnected SWCNT significantly shows at Figure 2.6. b, c) through GCD curves that represent stable performance at high scan rate compared to 3DGNs electrode, especially above the charge-discharge current density of 20 A/g. The i-3DGNs possesses a higher capacitance value with a multidimensional nanostructure that improves electrical conductivity and minimizes the electrical loss via 3DGNs and maintains electrochemical activity such as wettability and charge transport. The specific capacitance values are exhibited 371, 363, 340, 312, 289, 278 F/g at the scan rate of 2, 5, 10, 20, 50, 100 A/g, respectively. The rate capability retains 84.5% at 20 A/g (comparing to 61% at 3DGNs) and even lasts the retention about 75% of the initial capacitance at 100 A/g, which certainly results the better rate capability of the as-prepared 3DGNs electrodes.

The Nyquist plot of the 3DGNs / i-3DGNs in Figure 2.6. d) exhibits a minor semicircle at the high frequency region and a respectively flat line in the medium region. The minor diameter of semicircle shows the low charge transfer resistance at the electrode and electrolyte interface. In addition, the almost vertical straight line at the medium frequency region also represents the low charge transfer resistance for the adsorption process that is significant influenced by the morphology on the electrode surface. The lower resistance of i-3DGNs compared to 3DGNs could be because of improving conductivity in the interconnected 3D nanostructure.

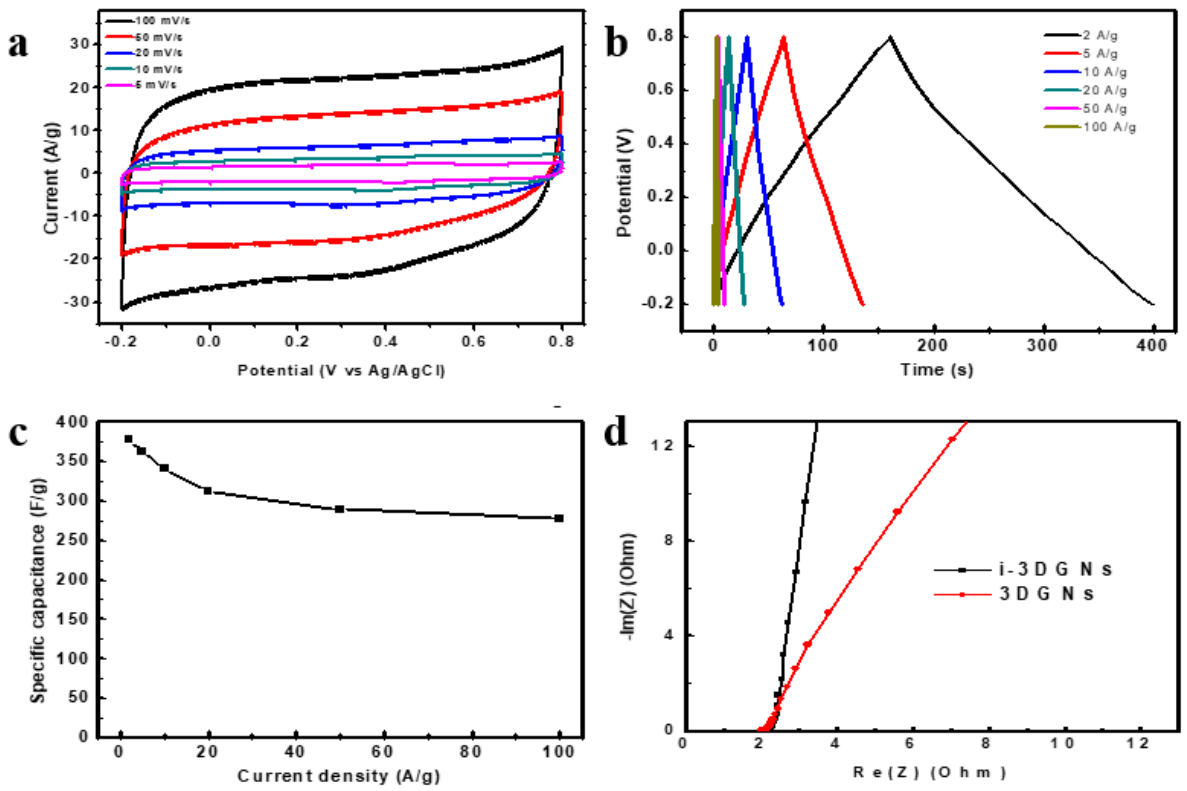

Figure 2.6. Electrochemical performance of i-3DGNs supercapacitors. (a) Cyclic voltammetry curves of i-3DNGs electrode at the scan rate of 5 to 100 mV/s. (b) Galvanostatic charge-discharge plots of 3DGNS at a current density of 2 A/g to 100 A/g. (c) Specific capacitance values as a wider range of current density compared to 3DGNs data. (d) Nyquist plot of i-3DGNs electrode in 1M H_2SO_4 electrolyte solution compared to 3DGNs

The fabrication of a settled and printable inks for commercial printer have to consider some rheological properties such as surface tension, viscosity, density of the printable solution and the size of the printer head. The physical properties of different inks were optimized to fulfill requirement of the printable inks, and then the inks are injected into a clean ink cartridge. To solve clogging of the cartridge head, each electrode for inks in IPA is subjected to centrifugation (at 3000rpm for 1 h) to remove large-sized particles and agglomerates before being filled into the cartridge. We initially focus on optimizing the viscosity of ink and surface tension like commercial inks in order to fabricate a proper ink for the inkjet printer. Because the viscosity for the commercial ink solution is about 2.0 cP, we control the ink of components to develop suitable ink, which contains two types of active materials, amount of solvent, surfactant at Figure 2.7. a, b, c). Initially, water is used as solvent, but it has relatively higher boiling point (100^{o}C), which, is hard to vaporize spontaneously after print. While isopropyl alcohol (IPA) as solvent (82.6^{o}C), which has a low boiling point compared to water, is useful for printing solution because it is quick to dry due to high vapor pressure and does not appear coffee ring effects, even though it is well dispersion solution and does not cause bubbles from surfactant unlike water[11,44]. Figure 2.7. d) shows the variation in the inks contact angle of the A4 paper substrates in a short term of time(~10s). On the A4 paper, each ink is quickly absorbed, of those commercial ink is absorbed the fastest, and negative / positive inks are absorbed more slowly because of the size of the active materials and other many impurities.

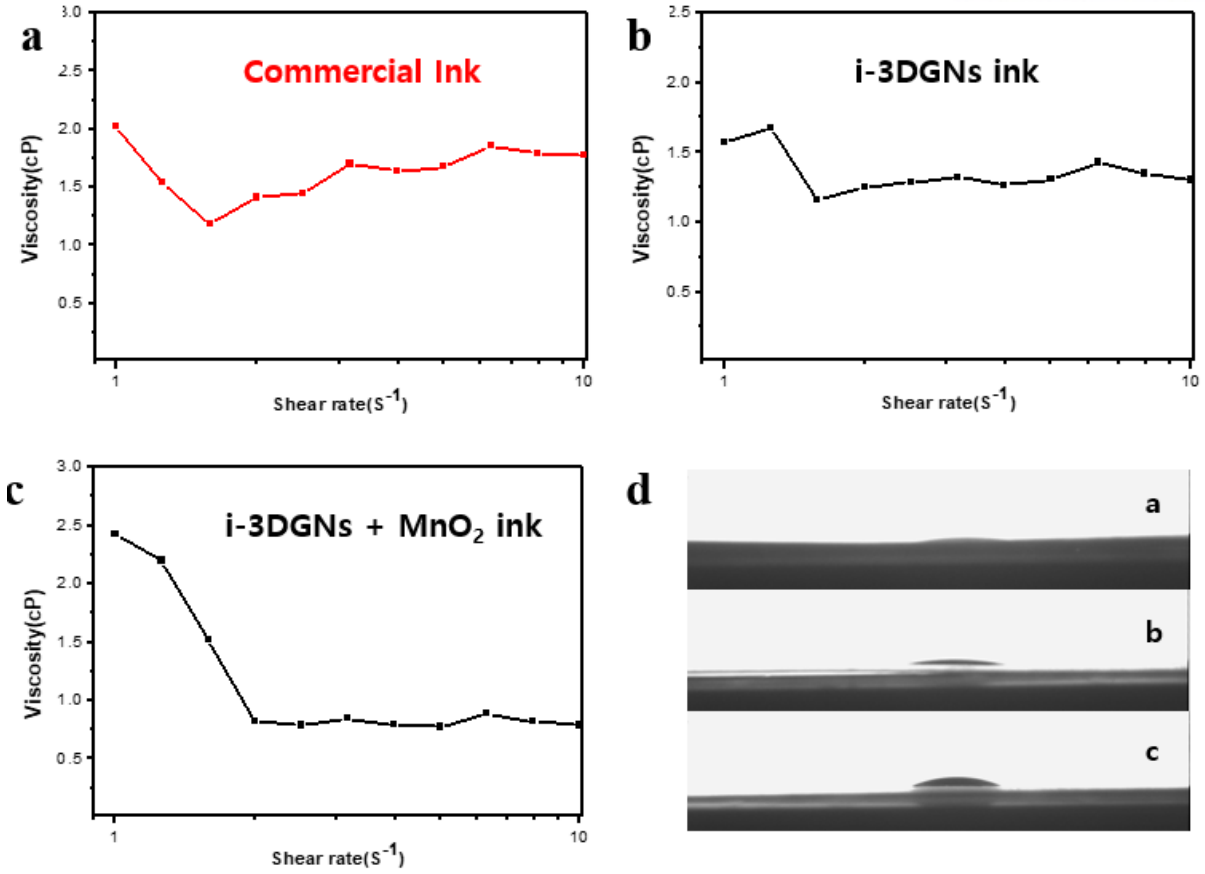

Figure 2.7. Rheological properties for each ink. The inks of commercial inks (a), i-3DGNs (b) and adding MnO_2 solution (c) at the various shear rate. The contact angle of different inks on an A4 paper substrate (d).

All the as-prepared different inks are shows to be significantly stable with well dispersion state in over 3 months at Figure 2.8. a). The as-bought SWCNT solution and prepared inks are filled into following colored cartridge: black – negative materials / yellow – positive materials / magenta – SWCNT solution acting as current collector. Figure 2.8. b, c) show various images of printed electrode and patterns with different shapes, sizes through setting of the photoshop or CAD, which could be used design the printed patters. Printing process is operated by selecting the high-quality and fast resolution mode.

Parts d, e in Figure 2.8. show comparative resistance versus numbers of printed layers for current collector and each printed electrode samples for SWCNT, negative and positive materials. With 35 times of printing layer, we obtain a sheet resistance of 16 ohm/sq, which is comparable to previous reported conducting paper by using lower cost than expensive metal materials. Because the paper can be curved over and over again in the process of printing, the drying procedure is pretty important to print a better quality of printed electrode, and also consider repeating at the same location of electrode to prevent the ink's spread phenomena between the narrow electrodes. At these process, each electrode has a sheet resistance of 16, 2.4 and 3.2 ohm/sq values, respectively SWCNT, negative and positive electrode.

The cross-section SEM image of the printed electrode has shown in Figure 2.9. the electrode components are deposited priorly on the surface of the A4 paper at Figure 2.9. a). Figure b) shows The thicknesses of the each electrodes are about 10 μm. Parts of c and d show a densely array of SWCNT layer at the bottom sites, where SWCNT is also interconnected between 3DGNs materials at the c) image, and d) image indicates well mixed MnO_2 in 3DGNs, and active materials are properly deposited on the current collector,

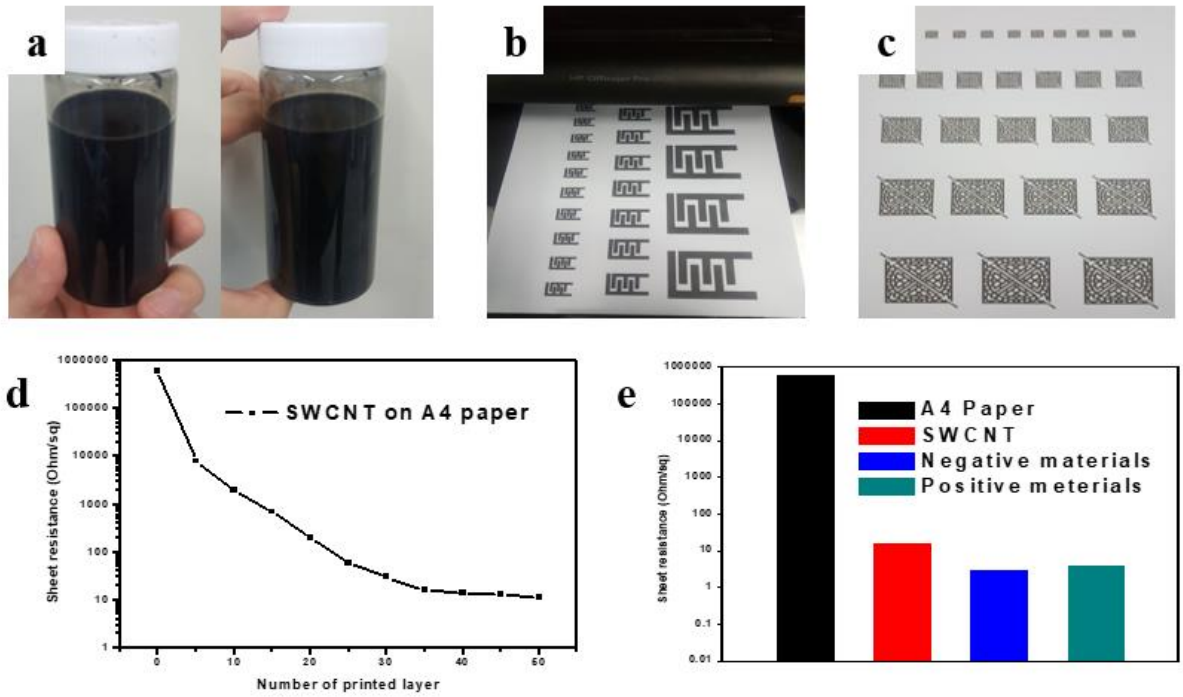

Figure 2.8. (a) Stable state of inks (left one: i-3DGNs is the negative ink / right one: i-3DGNs / MnO_2 is the positive ink, respectively). (b), (c) Various printing shape of the electrode (interdigitated and traditional shape) using HP Officejet Pro 8100 printer. (d) Sheet resistance vs. number of printed layer for SWCNT as current collector in A4 paper. (e) Comparison about sheet resistance of the printed electrodes on different materials by printing 35 times.

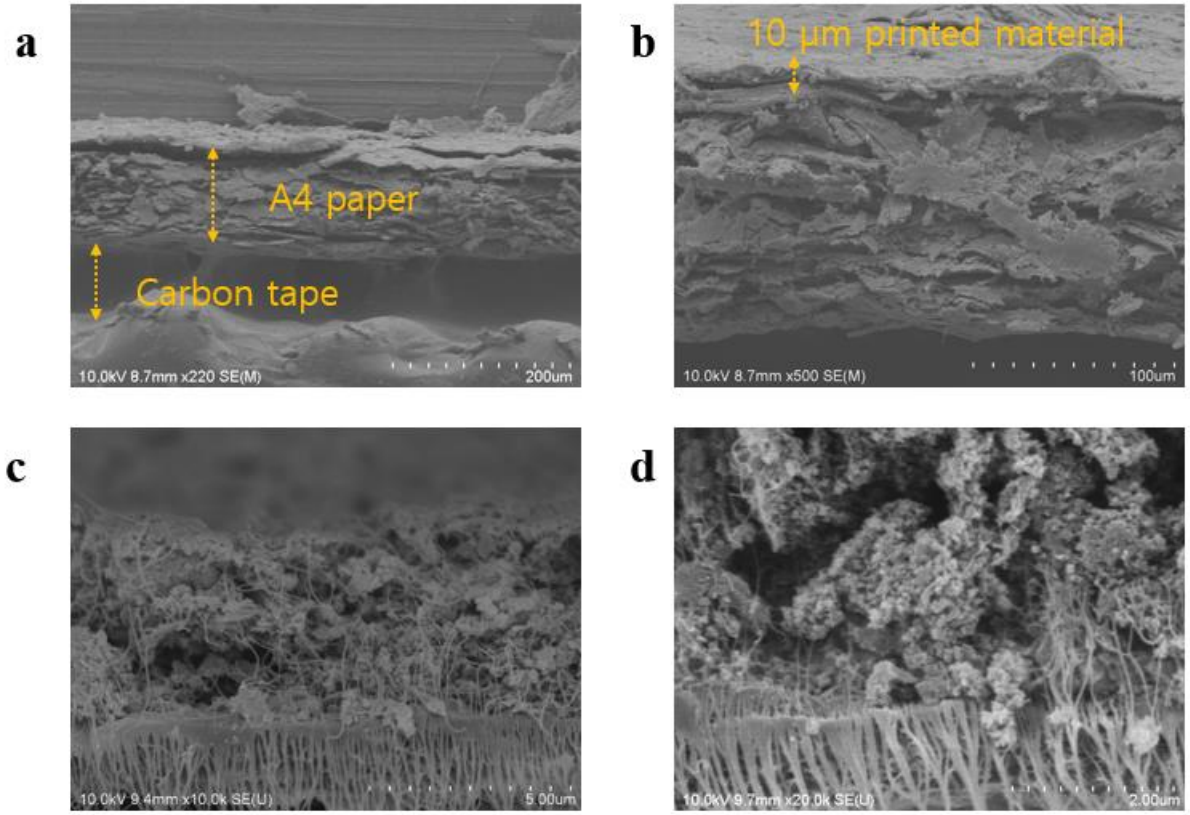

Figure 2.9. Cross-sectional SEM images of inkjet-printed paper by (a-c) i-3DGNs inks. (d) i-3DGNs / MnO_2 inks, show an arrangement of SWCNT layers at the bottom site, and each of active materials is well covered.

The solid-state PAS is fabricated by assembling PVA-LiCl gel electrolyte as separator at the same time. The as-prepared gel electrolyte is plastered on each electrode and solidified within 24hr at 45ºC oven. PAS device is packed with PET tape to prevent absorbed water in a gel. Figure 2.10. a) shows CV curves of the optimized PAS at different scan rates from 100 mV/s to 3 V/s. CV curves depict nearly rectangular shape and capacitive behavior without any redox peaks. The PAS devices are even retained under high scan rate of 3V/s, which demonstrates the fast charge/discharge properties. The CV curves of the negative and positive electrode with 35 printing numbers are indicated in Figure 2.10. b) at a variety of scan rate from 100 mV/s to 3 V/s, which has enlarged total potential window up to 1.8 V, Figure c) shows especially gradual extend of potential window from 0.8 V to 2.0 V at 100 mV/s. the wide potential window shows a large energy density that is a critical advantage compared to nomal symmetric supercapacitors and a major factor to satisfy the demand of various applications.

Moreover, the fabricated PAS shows excellent cyclic stability, which is carried out to evaluate the long cycle stability of GCD, a current density of 20 mA/cm^2 at Figure 2.10. d). Even though the capacitance has a minor change in the process of cell test, the capacity retention is 96.7% after 15,000 cycles and fully 91.4% after 50,000 cycles that infers the tremendous charge/discharge reversibility of devices due to stable characterization of i-3DGNs. Figure 2.10. e-f) shows CV curves of PAS at a scan rate 100 mV/s during various bending conditions such as 0º, 45º, 90º and 180º, which nearly overlap each other, with insignificant distortion and it is vital for the design of flexible and wearable devices about various application.

To highlight the specific functions of the A4 paper including the printable asymmetric supercapacitors as integrated power sources, we fabricate inter-digitate structural device that is aesthetically printable, designable and attachable versatile devices. Figure 2.11. a-b) shows the inter-digitated devices as well packed PET tape and bendable properties. This flexible supercapacitors from A4-based electrode, efficiently operated white LED ballpoint pen at 3.5 V, are much more valuable because it can be used in a multifarious aspect and lighter than a coin cell, as shown in Figure 2.11. c), suggesting the infinite potential of printable asymmetric supercapacitors in any portable and wearable device.

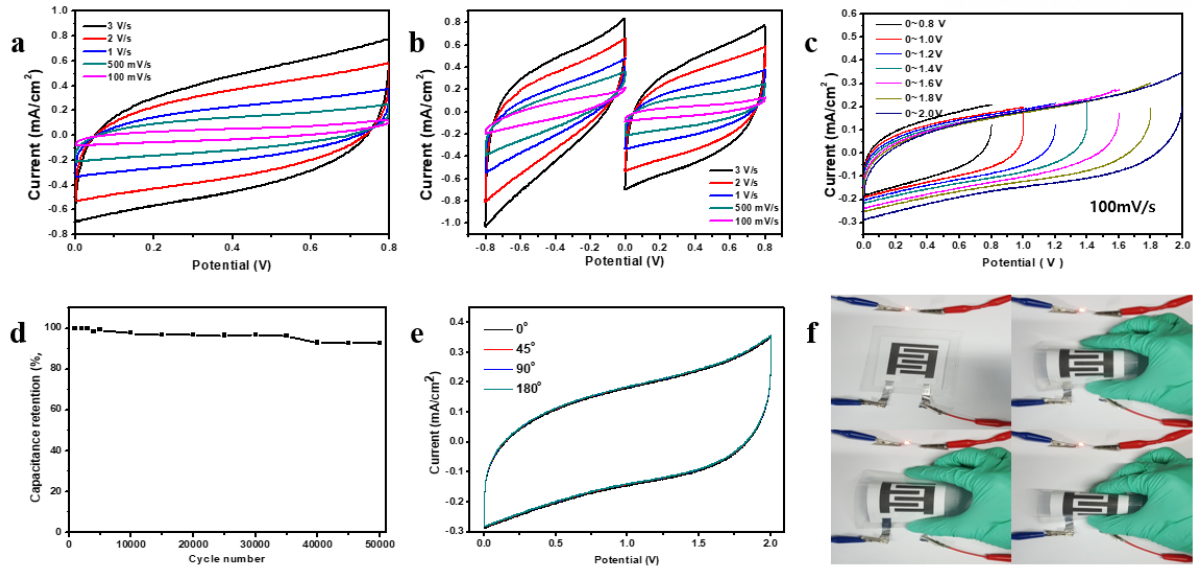

Figure 2.10. Electrochemical performances of the Printable asymmetric supercapacitors (PAS). (a) CV curves of an Optimized PAS at scan rate 100mV/s to 3V/s. (b) CV curves for negative and positive electrode at scan rate 100mV/s to 3V/s. (c) CV curves of PAS device measured at different voltage ranges at scan rate 100 mV/s. (d) Capacity retention of PAS with outstanding charge/discharge cycles. (e) CV curves of PAS at a scan rate 100 mV/s under various bending angles. (f) Photograph indicating the operation of the red LED under different bending angles.

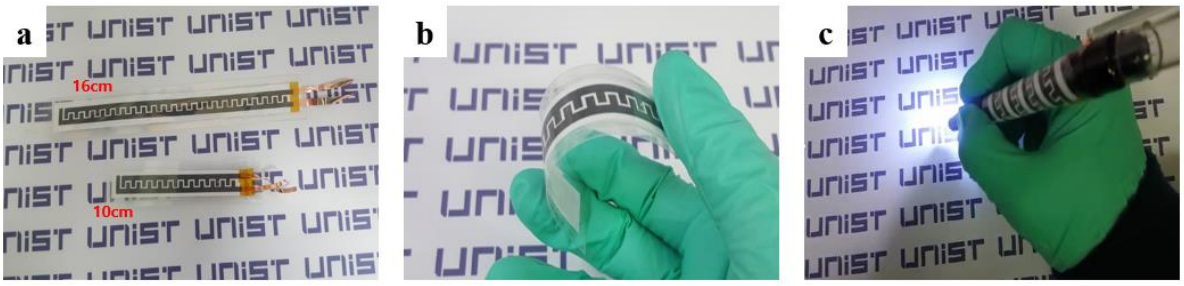

Figure 2.11. Photograph of PAS device depict (a) different size of devices. (b) showing the flexibility of PAS device. (c) operating LED ballpoint pen by PAS in series.

2.4 Conclusion

To sum up, we have completely demonstrated fabricating printable asymmetric supercapacitors on the A4 paper by using a facile printing method. The highly conducting patterns based on SWCNT as current collector, i-3DGNs and MnO_2 as active materials have been prepared by using commercial desktop printer. We have tried to fabricate facile printed devices to satisfy a few obstacles of versatile energy storage devices like low cost, flexibility, stability, light weight., resolve all of these problems by utilizing a facile and inexpensive A4 paper substrate and printed active layer of negative/positive electrode structures. Printed electrodes are put together by using PVA-LiCl gel polymer electrolyte as solid-state PASs and is packed with PET tape. This printed power sources show a large potential window up to 1.8 to 2.0 V and displays an outstanding electrochemical performance regardless bending angles and excellent cycle stability about 50,000. Furthermore, because PAS is aesthetically printable, designable and attachable through integration of inkjet printing process for flexible and wearable devices, which has infinite potential in a large range of applications to meet demands of flexible , portable and wearable energy storage electronics.

2.5 Reference

1. Bauer, Siegfried. *"Flexible electronics: Sophisticated skin." Nature materials* 12.10 (2013): 87
2. Gogotsi, Yury. *"Materials science: Energy storage wrapped up." Nature* 509.7502 (2014): 568
3. Xu, S., Zhang, Y., Cho, J., Lee, J., Huang, Cheng, H. "*Stretchable batteries with self-similar serpentine interconnects and integrated wireless recharging systems." Nature communications*, *4*, (2013): 1543.
4. Zhang, Yi-Zhou, et al. *"Flexible supercapacitors based on paper substrates: a new paradigm for low-cost energy storage." Chemical Society Reviews* 44.15 (2015): 5181-5199.
5. Zhou, Guangmin, Feng Li, and Hui-Ming Cheng. *"Progress in flexible lithium batteries and future prospects." Energy & Environmental Science* 7.4 (2014): 1307-1338.
6. Yan, Chaoyi, and Pooi See Lee. *"Stretchable energy storage and conversion devices." Small* 10.17 (2014): 3443-3460.
7. Ok, Jong G., et al. *"Photo–roll lithography (PRL) for continuous and scalable patterning with application in flexible electronics." Advanced materials* 25.45 (2013): 6554-6561.
8. Schumm, Benjamin, et al. *"Semi-transparent silver electrodes for flexible electronic devices prepared by nanoimprint lithography." Journal of Materials Chemistry C* 1.4 (2013): 638-645
9. Jang, Jingon, et al. *"The application of orthogonal photolithography to micro-scale organic field effect transistors and complementary inverters on flexible substrate." Applied Physics Letters* 104.5 (2014): 24_1
10. Chiolerio, Alessandro, et al. *"Ag nanoparticle-based inkjet printed planar transmission lines for RF and microwave applications: considerations on ink composition, nanoparticle size distribution and sintering time." Microelectronic Engineering* 97 (2012): 8-15.
11. Choi, Keun-Ho, et al. "All-inkjet-printed, solid-state flexible supercapacitors on paper." *Energy & Environmental Science*9.9 (2016): 2812-2821
12. Wang, Siliang, et al. "Inkjet printing of conductive patterns and supercapacitors using a multi-walled carbon nanotube/Ag nanoparticle based ink." *Journal of Materials Chemistry A* 3.5 (2015): 2407-2413..
13. Sundriyal, Poonam, and Shantanu Bhattacharya. "Inkjet-Printed Electrodes on A4 Paper Substrates for Low-Cost, Disposable, and Flexible Asymmetric Supercapacitors." *ACS applied materials & interfaces* 9.44 (2017): 38507-38521
14. Fromm, J. E. "Numerical calculation of the fluid dynamics of drop-on-demand jets." *IBM Journal of Research and Development* 28.3 (1984): 322-333.

15. Jang, Daehwan, Dongjo Kim, and Jooho Moon. "Influence of fluid physical properties on ink-jet printability." *Langmuir* 25.5 (2009): 2629-2635.

16. Van Osch, Thijs HJ, et al. "Inkjet printing of narrow conductive tracks on untreated polymeric substrates." *Advanced Materials* 20.2 (2008): 343-345.

17. Ma, Siyuan, et al. "Fabrication of novel transparent touch sensing device via drop-on-demand inkjet printing technique." *ACS applied materials & interfaces* 7.39 (2015): 21628-21633.

18. Rieu, Mathilde, et al. "Inkjet printed SnO2 gas sensor on plastic substrate." *Procedia engineering* 120 (2015): 75-78.

19. Qin, Yiheng, et al. "Inkjet Printing of a Highly Loaded Palladium Ink for Integrated, Low-Cost pH Sensors." *Advanced Functional Materials* 26.27 (2016): 4923-4933.

20. Liu, Libin, et al. "Wearable energy-dense and power-dense supercapacitor yarns enabled by scalable graphene–metallic textile composite electrodes." *Nature communications* 6 (2015): 7260

21. Xia, H.; Zhu, D. D.; Luo, Z. T.; Yu, Y.; Shi, X. Q.; Yuan, G. L.; Xie, J. P., Hierarchically Structured Co3O4@Pt@MnO2 Nanowire Arrays for High-Performance Supercapacitors. *Sci Rep-Uk* **2013,** *3*.

22. Lang, J. W.; Kong, L. B.; Wu, W. J.; Liu, M.; Luo, Y. C.; Kang, L., A facile approach to the preparation of loose-packed Ni(OH)(2) nanoflake materials for electrochemical capacitors. *J Solid State Electr* **2009,** *13* (2), 333-340.

23. Li, Qi, et al. "Design and synthesis of MnO2/Mn/MnO2 sandwich-structured nanotube arrays with high supercapacitive performance for electrochemical energy storage." *Nano letters* 12.7 (2012): 3803-3807.

24. He, Yongmin, et al. "Freestanding three-dimensional graphene/MnO2 composite networks as ultralight and flexible supercapacitor electrodes." *ACS nano* 7.1 (2012): 174-182.

25. Geim, Andre K., and Konstantin S. Novoselov. "The rise of graphene." *Nature materials* 6.3 (2007): 183.

26. Novoselov, Kostya S., et al. "Electric field effect in atomically thin carbon films." *science* 306.5696 (2004): 666-669.

27. Yoon, Jong-Chul, et al. "Three-dimensional graphene nano-networks with high quality and mass production capability via precursor-assisted chemical vapor deposition." *Scientific reports* 3 (2013): 1788

28. Lee, Jung-Soo, et al. "Chemical vapor deposition of mesoporous graphene nanoballs for supercapacitor." *ACS nano* 7.7 (2013): 6047-6055.

29. Waterhouse, Geoffrey IN, and Mark R. Waterland. "Opal and inverse opal photonic crystals: fabrication and characterization." *Polyhedron* 26.2 (2007): 356-368.

30. Hatton, Benjamin, et al. "Assembly of large-area, highly ordered, crack-free inverse opal films." *Proceedings of the National Academy of Sciences* 107.23 (2010): 10354-10359.

31. Ji, Hengxing, et al. "Graphene growth using a solid carbon feedstock and hydrogen." *ACS nano* 5.9 (2011): 7656-7661.

32. Merel, P., et al. "Direct evaluation of the sp3 content in diamond-like-carbon films by XPS." *Applied Surface Science*136.1-2 (1998): 105-110.

33. Jiang, Rongrong, et al. "Factors influencing MnO2/multi-walled carbon nanotubes composite's electrochemical performance as supercapacitor electrode." *Electrochimica acta* 54.27 (2009): 7173-7179.

34. Sundriyal, Poonam, and Shantanu Bhattacharya. "Inkjet-Printed Electrodes on A4 Paper Substrates for Low-Cost, Disposable, and Flexible Asymmetric Supercapacitors." *ACS applied materials & interfaces* 9.44 (2017): 38507-38521

35. Zhou, J.; Lian, J.; et al, *"Ultrahigh volumetric capacitance and cyclic stability of fluorine and nitrogen co-doped carbon microspheres." Nature communications* **2015,** *6*, 8503.

36. Qie, L.; Chen, W, et al, *"Synthesis of functionalized 3D hierarchical porous carbon for high-performance supercapacitors." Energy & Environmental Science* **2013,** *6* (8), 2497-2504.

37. Miyasaka, Y. N., Atsushi; Temmyo, Jiro. *"Graphite Thin Films Consisting of Nanograins of Multilayer Graphene on Sapphire Substrates Directly Grown by Alcohol Chemical Vapor Deposition." JPN J. Appl. Phy.* 2011, 50, 04DH12.

38. Ferrari, A.; Meyer, J, *"Raman spectrum of graphene and graphene layers." Physical review letters* **2006,** *97* (18), 187401.

39. Chaudhari, Nitin Kaduba, Min Young Song, and Jong-Sung Yu. "Heteroatom-doped highly porous carbon from human urine." *Scientific reports* 4 (2014): 5221.

40. Wei, W.; Liang, H, *"Nitrogen-doped carbon nanosheets with size-defined mesopores as highly efficient metal-free catalyst for the oxygen reduction reaction." Angewandte Chemie* **2014,** *53* (6), 1570-4.

41. Zhang, J.; Zhao, Z.; Xia, Z.; Dai, L., *"A metal-free bifunctional electrocatalyst for oxygen reduction and oxygen evolution reactions." Nature nanotechnology* **2015,** *10* (5), 444-52.

42. Fantini, C., et al. "Optical transition energies for carbon nanotubes from resonant Raman spectroscopy: Environment and temperature effects." *Physical review letters* 93.14 (2004): 147406.

43. Souza Filho, A. G., et al. "Stokes and anti-Stokes Raman spectra of small-diameter isolated carbon nanotubes." *Physical Review B* 69.11 (2004): 115428.

44. Kuang, Minxuan, Libin Wang, and Yanlin Song. "Controllable printing droplets for high-resolution patterns." *Advanced materials* 26.40 (2014): 6950-6958.